International Journal of Civil Engineering
https://doi.org/10.1007/s40999-018-0369-x

RESEARCH PAPER

Two-Dimensional Dynamic Analysis of Alluvial Valleys Subjected to Vertically Propagating Incident SH Waves

Atefeh Nohegoo-Shahvari[1] · Mohsen Kamalian[2] · Mehdi Panji[3]

Received: 21 May 2018 / Revised: 28 September 2018 / Accepted: 29 October 2018

Abstract
This study presents the formulation of a finite-element numerical method for the analysis of shear wave dispersion out of plane SH. Also, it evaluates the seismic behavior of alluvial valleys located in a semi-infinite rigid space. This formulation is implemented in computer codes in time domain. To examine the accuracy of the program, various examples are solved and some numerical considerations in the dynamic analysis of the topographic feature are investigated by parametric studies. The results indicate that the appropriate time step in the finite-element method (FEM) is 45/1000 of the predominant period of the incident wave. The appropriate length of the element should be selected for placing at least eight nodes on the smallest wavelength. Increasing Gaussian points in integrating mass matrices in comparison with stiffness matrices is not effective in the accuracy of results. It was found that the choice of $\delta > 0.5$ in Newmark's integration method reduced the amplitude, but the change in the α value did not affect the results. The effect of a feature on the ground response is only noticeable if the wavelengths are comparable with the dimensions of the feature.

Keywords FEM · SH waves · Element length · Time step · Coefficients of Newmark's integration · Gaussian points (GPs)

1 Introduction

Topographic feature plays a critical role in seismic destructions. Besides, the tendency of societies to develop urban fabric near these sites has made this issue more important. For this reason, researchers have proposed several methods to provide quantitative and qualitative definitions for estimating these effects. One of the important topographic features is the study of the seismic behavior of alluvial valleys subjected to propagating incident SH waves. Initially, the researchers used analytical methods to study the effects of topography, while Trifunac [1, 2] developed an evolution in analytical methods and using the Bessel series solved a two-dimensional modeling of circular and submerged alluvial valleys under SH waves. In the following years, several researchers evaluated analytical and semi-analytical methods to investigate the problem of SH elastic wave dispersion in alluvial valleys [3–8]. Specifically, some of Tsaur's research can be pointed out [9–12]. This research conducted several studies such as analysis of partially filled semi-circular alluvial valley, truncated semi-circular canyon, deep triangular valley, and partially filled semi-elliptical alluvial valley using region-matching method. Due to desirable accuracy in the results of analytical and semi-analytic methods, researchers are still developing these methods; however, a low flexibility and limited application of these methods in some specific and simple cases of topographic features have directed researchers to numerical methods. Numerical methods that are divided into three groups of volumetric, boundary and combined methods are more compatible with nature and have the ability to model topographic features with complex geometries.

✉ Mohsen Kamalian
Kamalian@iiees.ac.ir

Atefeh Nohegoo-Shahvari
a.nohegoo92@iau-arak.ac.ir

Mehdi Panji
m.panji@iauz.ac.ir

[1] Department of Civil Engineering, Arak Branch, Islamic Azad University, Arak, Iran

[2] Geotechnical Engineering Research Center, International Institute of Earthquake Engineering and Seismology (IIEES), No. 26, Arghavan Street, North Dibajee, Farmanieh, Tehran, Iran

[3] Department of Civil Engineering, Zanjan Branch, Islamic Azad University, Zanjan, Iran

Published online: 07 November 2018

Finite-element method (FEM), finite difference method (FDM), and spectral finite-element method (SFEM) are the most familiar volumetric methods. In volumetric methods, the domain of the studied environment is discontinued, and the governing boundary conditions such as the conditions for the emission of waves in an infinite space are established by defining a series of approximate energy-absorbing boundaries around the desired region [13]. This method typically focuses on investigating the seismic behavior of alluvial valleys under propagating incident SV and P waves [14–18]. Therefore, the technical literature shows few studies on the evaluation of the seismic behavior of SH wave-exposed alluvial valleys using volumetric methods. This approach was only used by Bielak [19] and Gelagoti [20]. Bielak [19] has examined the seismic response of a small valley in Kirovakan during an earthquake in Armenia 1988. He presented a method for visualizing the structure response as a function of the natural-frequency simulator of the structure and its location within the valley. This method identifies a variety of potentially damaging structures and identifies situations within the valley that are likely to be highly damaged. He indicated that the simulation of two-dimensional ground motion offers a good description of the damage observed compared to the one-dimensional analysis. In the two-dimensional simulation, the maximum ground and structural response was predicted in the frequency range of 2.5–4.5 Hz, which is exactly in accordance with the natural frequencies of the four- to five-story structures that have experienced the great earthquake. Gelagoti [20] conducted a numerical study to evaluate the behavior of a shallow soft valley as a test case. In this study, the sensitivity of the two-dimensional valley response to parameters such as frequency of the input motion, its details and nonlinear behavior of the soil were investigated. The researcher indicated that the focus of the wave at the edges of the valley and the origin of the surface waves at the valley corners is responsible for significant aggravation of the seismic motion. Furthermore, he showed that applying non-linear soil behavior in calculating, the response of two-dimensional valleys in a measurable extent is correct, and increasing the damping ratio mainly affects the emission of surface wave.

The boundary methods have been developed to analyze linear elastic environments. They have been used by several researchers to evaluate the seismic motion of valleys and alluvial sites subjected to propagating incident SH waves [21–31], because of their ability to solve the problem by meshing geometric boundary of the object. In most of these researches, the effects of feature geometry (semi-circle, trapezoidal, and triangle), the ratio of impedance between alluvial and the surrounding area, and the need for 3D modeling of topographic features have been investigated. The third group of numerical methods is hybrid method. To enjoy the advantages of various methods, researchers aim to combine volumetric and boundary methods. Among conducted studies in this field, one can name the studies of Bielak [32], Gil-Zepeda [33], and Shyu [34].

As literature review showed, limited research has been conducted in the field of evaluating the seismic behavior of alluvial valley under propagating SH waves using FEM. Therefore, numerous questions in this field have remained unanswered. For example, is it possible to present a relationship to determine the length of element and appropriate time step? Does the increase in the order of integral mass matrix, compared to the stiffness matrix, affect the accuracy of the results? How do Newmark coefficients (NCs) affect the results of the problem in different damped and undamped conditions? How is the effect of the shape (height to half width) on magnification potential and frequency characteristics? Therefore, in this paper, we intend to use the time domain FEM to numerically investigate the dynamic aspects of this topographic feature. Accordingly, first, formulation of FEM is performed for the 2D dynamic analysis of a rectangle-shaped alluvial valley in a semi-finite rigid environment subjected to propagating incident SH waves. Then proper answers are provided for the questions above.

2 Problem Formulation

In this section, the formulation governing the problem and its matrix form are presented. Given that in the propagation of incident SH waves the displacement occurs perpendicular to the direction of propagation and out of plane, we present differential (scalar wave) equation in an isotropic, elastic, and homogeneous environment with a small displacement range as follows [35]:

$$\nabla^2 u + F = \frac{1}{c^2}\frac{\partial^2 u}{\partial t^2}, \tag{1}$$

where u is displacement out of plane, c is the shear wave velocity equivalent to $\sqrt{\frac{\mu}{\rho}}$, ρ is density, μ is shear modulus, and F is a volumetric force out of plane. Equation 1 is extracted from an elastic environment using the weighted residual method and weak formulation, where σ_{ij}, ε_{ij}, and t_i are tensor components of stress, strain, and traction on the boundary, respectively,

$$\int_{\Omega} \rho \ddot{u}_i \delta u_i \mathrm{d}\Omega + \int_{\Omega} \sigma_{ij} \delta \varepsilon_{ij} \mathrm{d}\Omega = \int_{\Gamma} t_i \delta u_i \mathrm{d}\Gamma + \int_{\Omega} F_i \delta u_i \mathrm{d}\Omega. \tag{2}$$

Then the equilibrium equation of enclosed area Ω is calculated as follows (where M is a mass matrix, K is stiffness matrix, C is damping matrix and R is the sum of surface and volumetric forces) [36]:

$$M\ddot{U} + C\dot{U} + KU = R. \tag{3}$$

In the present study, Rayleigh damping mechanism, which is proportional to the mass and stiffness matrices of the examined environment, is expressed as follows:

$$C = \beta_0 M + \beta_1 K, \tag{4}$$

where β_0 and β_1 are Rayleigh damping coefficients and are determined using the damping ratio ξ_i and at least two vibrational frequencies ω_i. The relationship between parameters β_0, β_1, ξ_i and ω_i is defined as follows:

$$\beta_0 + \beta_1 \omega_i^2 = 2\omega_i \xi_i. \tag{5}$$

2.1 Modification of Equilibrium Equation for Earthquake Input

In many seismic problems, loading is applied as a set of specific boundary accelerations; and does not include surface and volumetric forces. Hence, all points with certain accelerations are supposed to move together, which is represented by the acceleration–time history $\{\ddot{u}_g\}$. Now, if the system moves as a rigid body, every point will have the time history of motion which is defined by the vectors $\{u_g\}$, $\{\dot{u}_g\}$, and $\{\ddot{u}_g\}$. Here, $\{\dot{u}_g\}$ and $\{u_g\}$, respectively, are the results of one- and two-time integral of $\{\ddot{u}_g\}$ in time. In fact, the flexible mode is defined by relative movements between free nodes and nodes on a boundary that have a given motion, which is characterized by $\{V\}$, $\{\dot{V}\}$, and $\{\ddot{V}\}$ vectors [37]:

$$\begin{aligned} \{V\} &= \{U\} - \{u_g\} \\ \{\dot{V}\} &= \{\dot{U}\} - \{\dot{u}_g\} \\ \{\ddot{V}\} &= \{\ddot{U}\} - \{\ddot{u}_g\}. \end{aligned} \tag{6}$$

By placing Eq. 6 in 3, Eq. 7 is obtained, where $\{u_g\}$ describes rigid body motion. Since there are no direct forces in the calculation except $\{\ddot{u}_g\}$, the value of R is considered to be zero:

$$M\left(\{\ddot{V}\} + \{\ddot{u}_g\}\right) + C\{\dot{V}\} + K\{V\} = 0. \tag{7}$$

This formulation is widely used in earthquake engineering in relative motion terms. However, it should be noted that the freedom degrees of the formulation belong to the nodes with no specific time history of acceleration and relative displacement of these nodes remains in matrix $\{V\}$, which results in significant decrease in dimensions of matrices and vectors.

2.2 Algorithm

To solve differential equations, various numerical methods have been presented in their selection; two factors including stability and accuracy play an important role. Among these methods, Newmark's integration method which was used in the present study can meet both factors. In this method which is used as an expansion of linear acceleration, α and δ are parameters that can be determined to obtain the accuracy and stability of integration [36]. Also, Δt parameter, which is a time step, plays an important role in the volume and accuracy of calculations.

By re-writing Eq. 7 in $(t + \Delta t)$ time and using the Newmark's integration method, the FEM equation governing equilibrium of enclosed area is written as follows:

$$\overline{K}_{\mathrm{EF}} \cdot \{V^{t+\Delta t}\} = Z_{\mathrm{EF}}^{t+\Delta t}, \tag{8}$$

where

$$\begin{aligned} \overline{K}_{\mathrm{EF}} &= K + C\frac{\delta}{\alpha \Delta t} + M\frac{1}{\alpha \Delta t^2}, \\ Z_{\mathrm{EF}}^{t+\Delta t} &= -C\left[\{\dot{V}^t\} + \left((1-\delta)\{\ddot{V}^t\} + \frac{\delta}{\alpha} A_{\mathrm{EF}}^t\right)\Delta t\right] - M\left[A_{\mathrm{EF}}^t \frac{1}{\alpha} + \{\ddot{u}_g\}\right], \\ A_{\mathrm{EF}}^t &= -\left(\{V^t\} + \{\dot{V}^t\}\Delta t\right)\frac{1}{\Delta t^2} - \left(\frac{1}{2} - \alpha\right)\{\ddot{V}^t\}. \end{aligned} \tag{9}$$

In the next section, an algorithm is proposed to solve Eq. 8.

3 Flowchart

To analyze the dynamical responses of 2D environments under SH seismic waves, rigid bed rock FEM (RBRFEM) software is provided by considering elastic behaviors based on FEM. Deformation and accelerations are calculated by the software. In the part of the FEM, eight-node elements are used and the current program is rewritten by MATLAB software.

3.1 Introducing Subprograms

All main subprograms are called under MAIN PROGRAM tittle. Management of time steps and running of the program are done by this page. In the following, subprograms called by MAIN PROGRAM are introduced based on the priority of the call.

– WRITE DATA Subprogram

The main data of the problem are applied through this subprogram, which includes material properties, geometric type of feature, and the characteristics of the Ricker wavelet function. Besides, in this program, matrices of acceleration and free motion of the ground's surface are provided. The program is basically assigned to make the input file.

– INPUT DATA Subprogram

This subprogram reads the input file based on the WRITE DATA subprogram, in the order of the values printed in it and places it in the main variables of the program.

– COMPUT KMD Subprogram

In this subprogram, total stiffness, mass, and damping matrices of alluvial valleys are assembled. Then stiffness matrix of all materials $\overline{K}_{\mathrm{EF}}$ is formed based on Eq. 9.

– COMPUT ZF Subprogram
– This subprogram which is needed to be called by time step counter in each time step makes the matrix $Z_{\mathrm{EF}}^{t+\Delta t}$ based on Eq. 9. This matrix estimates and combines the node forces of the matrix related to the effects of previous steps and node forces such as damping and mass matrices, as well as the force resulting from the acceleration of the bedrock.
– COMPUT VRM Subprogram

In this subprogram, after applying boundary conditions, the equations are solved and relative displacement of each node in time of $(t + \Delta t)$ is computed. Then, in mentioned time, relative acceleration and velocity of each node are calculated and saved in memory.

– COMPUT U Subprogram

In this subprogram, by summing the value of acceleration and relative displacement of each node per time step with acceleration and free movement of the ground, total acceleration and displacement are computed.

– OUTPUT DATA Subprogram

Printing of the results of the analysis in the desired time steps is done by this program.

To show the accuracy, efficiency, and capability of the mentioned method in the analysis of the topographic feature in the time domain, two numerical examples will be solved.

4 One-Dimensional Example

In this example, the 2D modeling approach is used to carry out analysis of a 1D site with a homogenous layer on rigid bedrock exposed to vertical propagating incident SH waves. The input motion was selected as the Ricker wavelet function type (Eq. 10):

$$F(t) = \left[1 - 2\left(\pi f_{\mathrm{p}}(t - t_0)\right)^2\right] e^{-\left(\pi f_{\mathrm{p}}(t-t_0)\right)^2}, \tag{10}$$

where f_{p}, t_0, and t are dominant frequency, time shift parameter, and the real axis of time, respectively. Based on Eq. 10, the displacement out of plane of the incident SH wave is calculated by the following equation:

$$\begin{aligned} u^{\mathrm{inc}}(x, y, t) &= A_{\max}\left[1 - 2\left(\frac{\pi f_{\mathrm{p}}}{2}\alpha^{\mathrm{inc}}\right)^2\right] e^{-\left(\frac{\pi f_{\mathrm{p}}}{2}\alpha^{\mathrm{inc}}\right)^2} H\left(t - \frac{r^{\mathrm{inc}}}{c}\right), \\ \alpha^{\mathrm{inc}} &= c\left(t - t_0\right) + r^{\mathrm{inc}}, \\ r^{\mathrm{inc}} &= -\sin\theta x + \cos\theta y, \end{aligned} \tag{11}$$

where u^{inc} is displacement of SH wave incidence, $A_{\max}$ is the maximum amplitude of the displacement time history, H is Heaviside function, α^{inc} is the phase of incident wave in r^{inc} position, t is the time, and c is the shear wave velocity (Fig. 1).

Table 1 presents the properties related to soil layer and the incident SH wave while Figs. 2 and 3, respectively, show displacement and acceleration time histories of the input wave.

First, to determine the proper dimensions of the 2D site which simulates the 1D site, the results obtained from the analysis of two models with dimensions of 5000 m × 50 m and 6000 m × 50 m are compared. In each of the models, 400 and 480 eight-node elements are meshed. This analysis is performed to select the suitable spacing between lateral boundaries to prevent the errors resulting from the wave reflected by the lateral boundaries on the central point of the ground surface and simulating the 1D condition of the ground. In this analysis, the time step and NCs are, respectively, 0.0125 s and $\alpha = 0.25$ and $\delta = 0.5$.

In Fig. 4, acceleration–time history resulting from the analysis of two models in a central point on the ground surface is drawn and two obtained curves are completely overlapped, suggesting adequate distance between two lateral

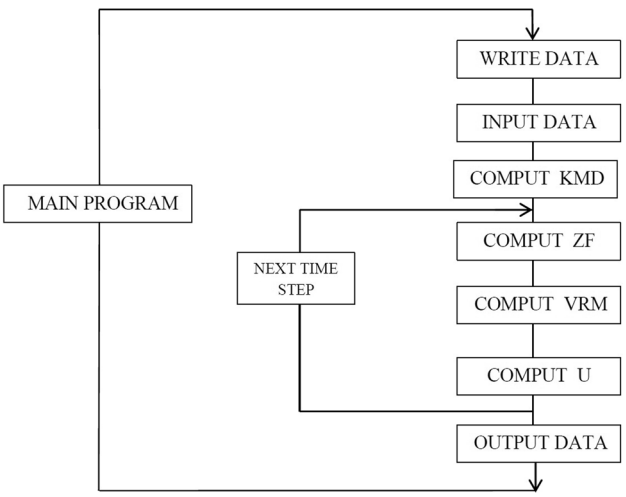

Fig. 1 Program flowchart

Table 1 Site and input wave properties of one-dimensional example

A_{max}(m)	f_p(Hz)	t_0(s)	ξ	Poisson ratio	$\rho\left(\mathrm{t}/\mathrm{m}^3\right)$	$\mu\left(\mathrm{kN}/\mathrm{m}^2\right)$
0.0001	2.4	0.9	0.05	1/3	2	180,000

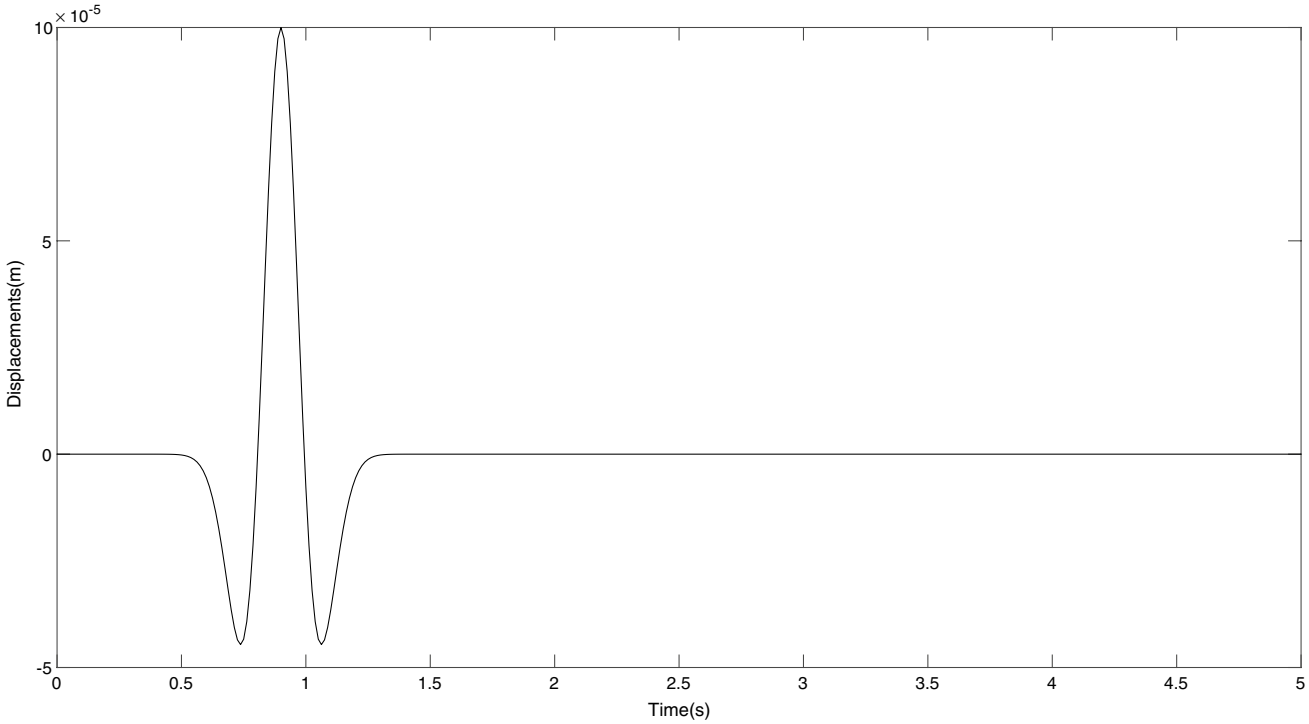

Fig. 2 Displacement of input SH wave in a point located at the flat surface of the ground in time domain

boundaries for simulation of the one-dimensional site. Then, to analyze the 1D site, a 6000 m width is considered.

In this step, as described earlier, a site with a depth of 50 m and width of 6000 m was evaluated (Fig. 5). In analyzing the site, 480 eight-node elements with 25 m × 25 m dimensions and 1925 nodes were used.

To verify the obtained results, an iso-parametric FEM program (i.e., Plaxis) is used to analyze the geotechnical problems. In Plaxis, this example was resolved with 15-node elements. To apply rigid boundary condition and seismic condition, lateral and bottom boundaries were exposed to the incident for the motion of input SH wave (Fig. 2). Figure 6 demonstrates the central point displacement of the site on the ground surface by analyzing FEM program of the present study and Plaxis software. As seen in Fig. 6, there is a good agreement between the results.

5 Two-Dimensional Example

To evaluate the efficiency and accuracy of this program in analyzing the two-dimensional problem, a rectangle-shaped valley (400 m × 200 m) located at a rigid half-space is analyzed. The assumed soil layer is homogeneous and uniform (Table 2). Also, 200 eight-node elements with 20 m × 20 m dimensions, with the total number of 661 nodes, and a 0.008-s time step is used.

To verify the problem, a half-plane BEM is used [30]. In this method, there is no need to define and discretize the ground surface to apply approximate boundary conditions because of the accurate governing boundary condition on the formulation. In fact, only the surface of the topographic or boundary surface of a structure, which is

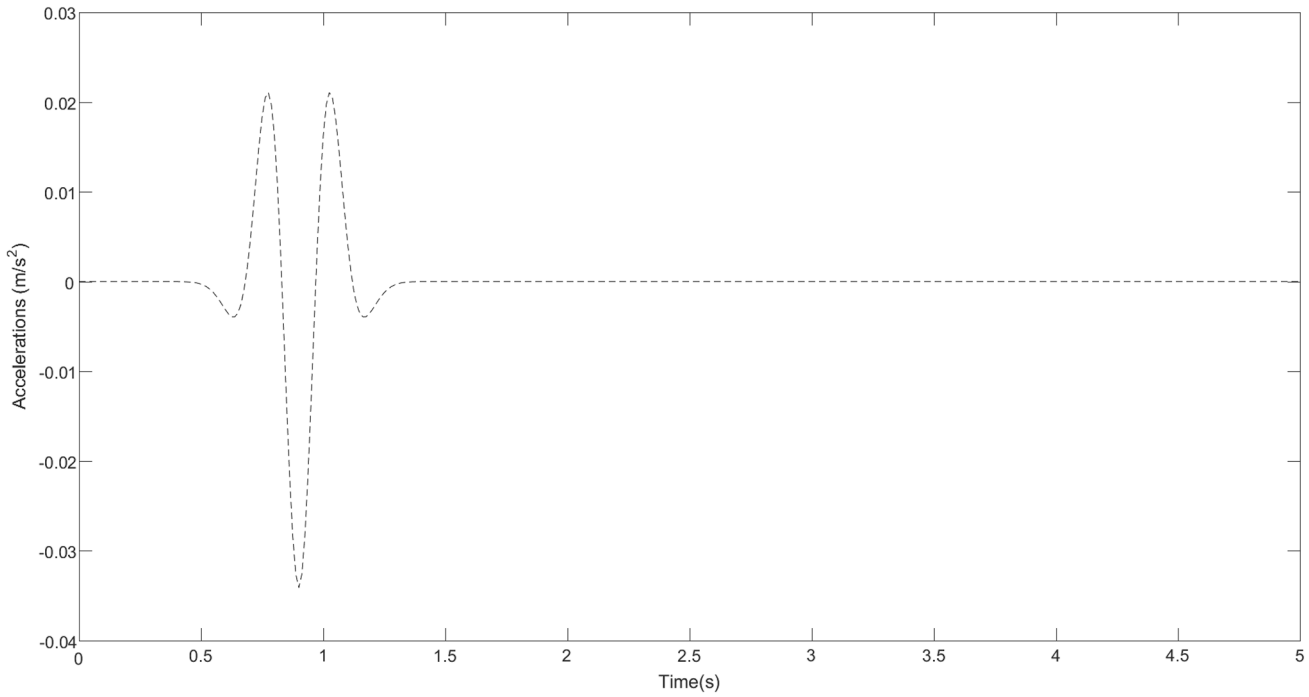

Fig. 3 The acceleration of input SH wave in a point located at the flat surface of the ground in time domain

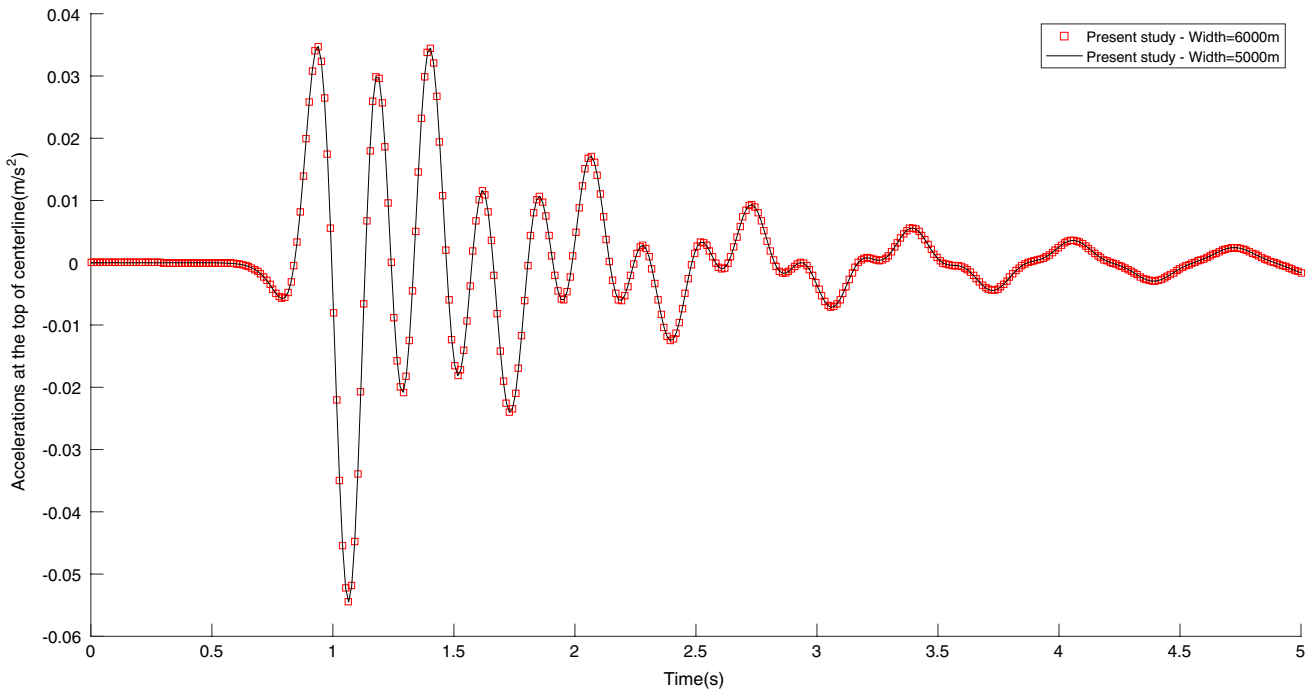

Fig. 4 The acceleration–time history of site's central point on the ground surface

related to some limits, is introduced into the modeling and eventually discretized. Therefore, when solving the propagating problem of SH waves to apply a seismic load, the reflecting wave component of the inverse phase should also be considered to satisfy the boundary conditions of the ground surface (Eq. 12):

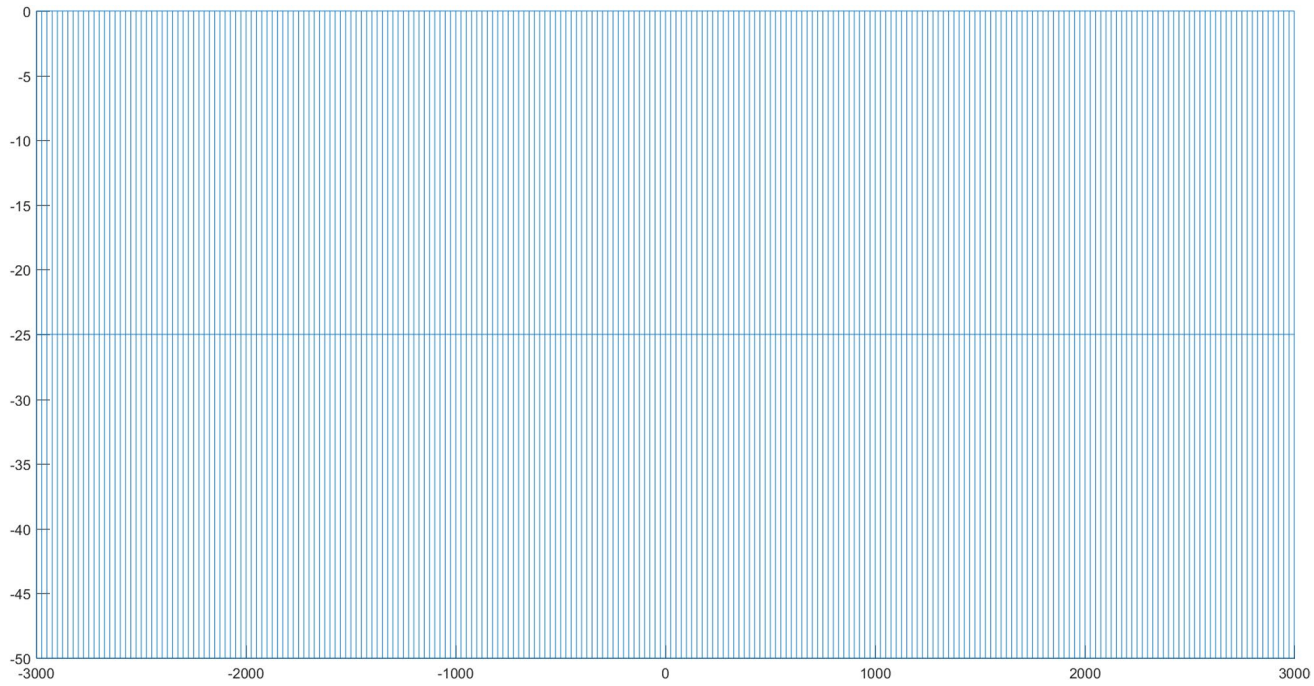

Fig. 5 Geometry and meshing the one-dimensional site on rigid bedrock

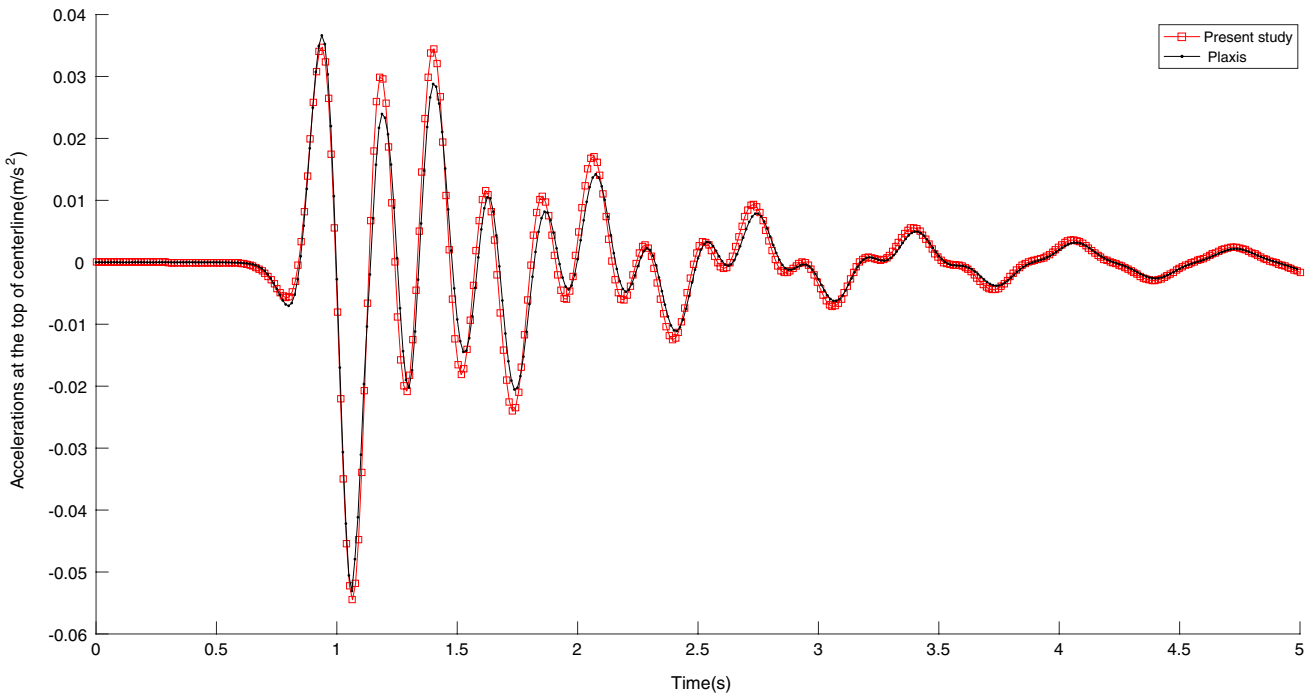

Fig. 6 Central point displacement of the site on the ground surface

Table 2 Characteristic of site and input wave in the two-dimensional example

A_{max}(m)	f_p(Hz)	t_0(s)	Poisson ratio	$\rho\left(t/m^3\right)$	$\mu\left(kN/m^2\right)$
0.001	3	1.7	1/3	2	320,000

$$u^{ref}(x,y,t) = A_{max}\left[1-2\left(\frac{\pi f_p}{2}\alpha^{ref}\right)^2\right]e^{-\left(\frac{\pi f_p}{2}\alpha^{ref}\right)^2}H\left(t-\frac{r^{ref}}{c}\right),$$
$$\alpha^{ref} = c\left(t-t_0\right)+r^{ref},$$
$$r^{ref} = -\sin\theta x-\cos\theta y, \tag{12}$$

where u^{ref} and α^{ref} are, respectively, displacement and reflexed wave phase from the ground surface in the position of r^{ref} and time of t. Finally, to calculate the displacement of the free field of ground surface u^{ff}, the following equation can be used:

$$u^{ff}(x,y,t) = u^{inc}(x,y,t)+u^{ref}(x,y,t). \tag{13}$$

The mentioned problem is modeled using the half-plane BEM. It is assumed that alluvium material and half-space are elastic, homogeneous, and isotropic. The shear modulus and alluvial density are represented by μ_2 and ρ_2, respectively, and the shear modulus and density of the half-space are μ_1 and ρ_1, respectively.

To simulate rigid boundary conditions in a half-plane BEM, several ratios of shear wave velocity are tested between half-space and alluvial materials $\left(\frac{c_1}{c_2}\right)$. Since in rigid boundary conditions, the points on the lateral and bottom boundaries should have the same time histories as input shear wave, this test is carried out to the extent that the results of the variations of the time history of the points on the boundary match the variations of the time history of the input wave (Table 3).

To compare the results of the tests, three points B, C, and D were selected on the lateral and bottom boundaries of the valley (Fig. 7), where the results of the displacement

Table 3 Characteristics of materials in half-plane BEM

	$\mu_1\left(kN/m^2\right)$	$\mu_2\left(kN/m^2\right)$	$\rho_1\left(t/m^3\right)$	$\rho_2\left(t/m^3\right)$	$\frac{c_1}{c_2}$
1	8.4×10^6	320,000	2.1	2	5
2	3.36×10^7	320,000	2.1	2	10
3	8.4×10^8	320,000	2.1	2	50
4	3.36×10^9	320,000	2.1	2	100
5	1.344×10^{10}	320,000	2.1	2	200
6	3.024×10^{10}	320,000	2.1	2	300

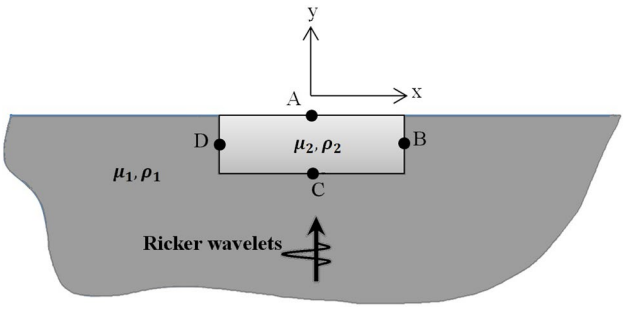

Fig. 7 Site geometry in the half-plane BEM

time histories for these points can be seen in Fig. 8. As can be seen, by increasing the velocity ratio between the materials in the valley and its surrounding, the displacements of the boundary points coincide and match with the displacement of the input wave's time history and finally, it is possible to provide the best conditions of the rigid boundaries at a velocity ratio of 300. Therefore, this velocity ratio is chosen to compare the results of BEM and FEM with rigid boundaries.

Another point that should be considered in the use of the half-plane BEM is that in very high velocity ratios, the valley acts like a cavity and the wave inside the valley is blocked, which leads to the undamped results. Therefore, to compare the results of two methods of half-plane BEM and FEM, the materials in the valley in the FEM program are considered undamped.

Totally, with the assumption of the NCs as $\alpha = 0.25$ and $\delta = 0.5$, the problem of the rectangular alluvial valley is solved by FEM and its results are compared at the central point on the ground (point A) with the results of the half-plane BEM. Figure 9 illustrates the results of the displacement time history of this point, indicating a good agreement of the results.

6 Parametric Studies

One of the important concerns in increasing the accuracy of the results of numerical methods, including FEM, is the proper selection of a number of parameters such as time step and element length. Therefore, in this study, the effect of these parameters is considered and a suitable relation for choosing these values is presented.

6.1 Element Length

In this research, a rectangle-shaped valley (400 m × 200 m) located in a rigid half-space is evaluated (Fig. 10). The soil layer is assumed uniformed and homogenous and its material is undamped. The results of this section are compared to

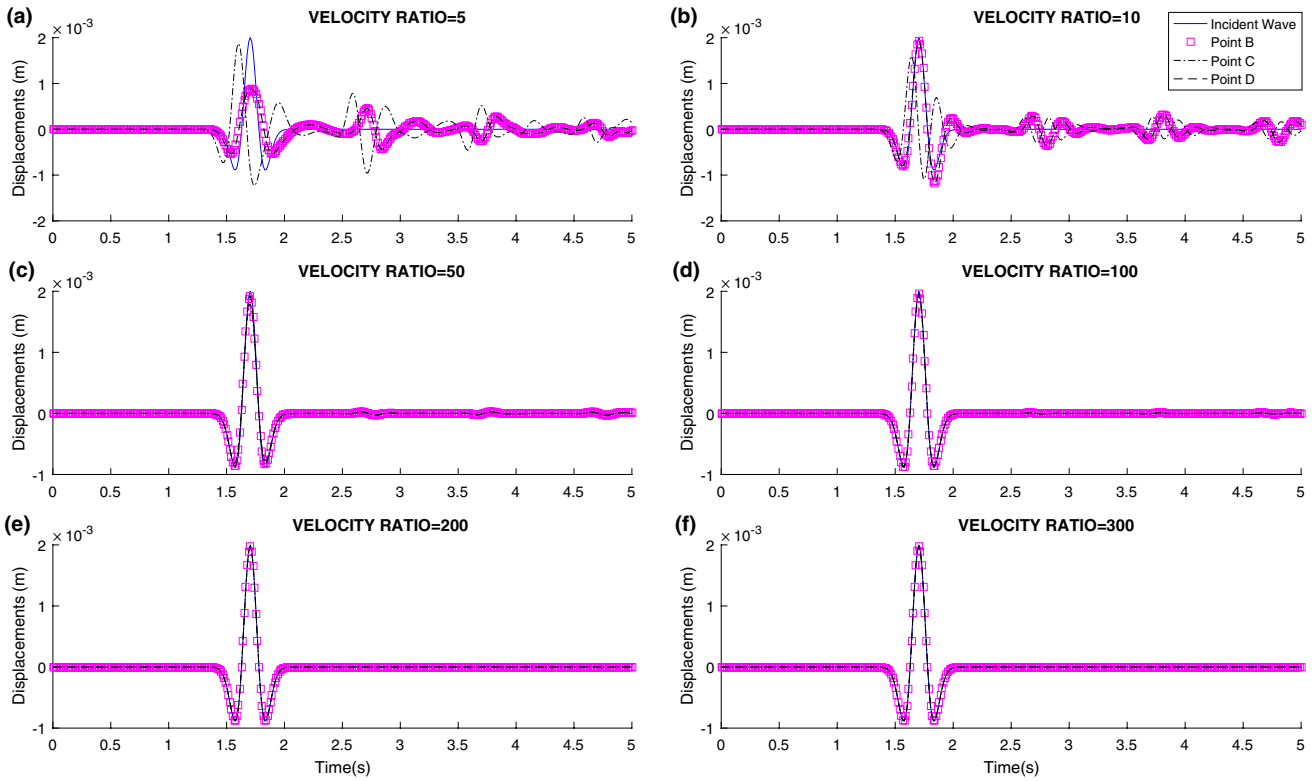

Fig. 8 Displacement time histories in points on the lateral and bottom boundaries compared with the displacement of the input wave's time history at a velocity of 400 m/s

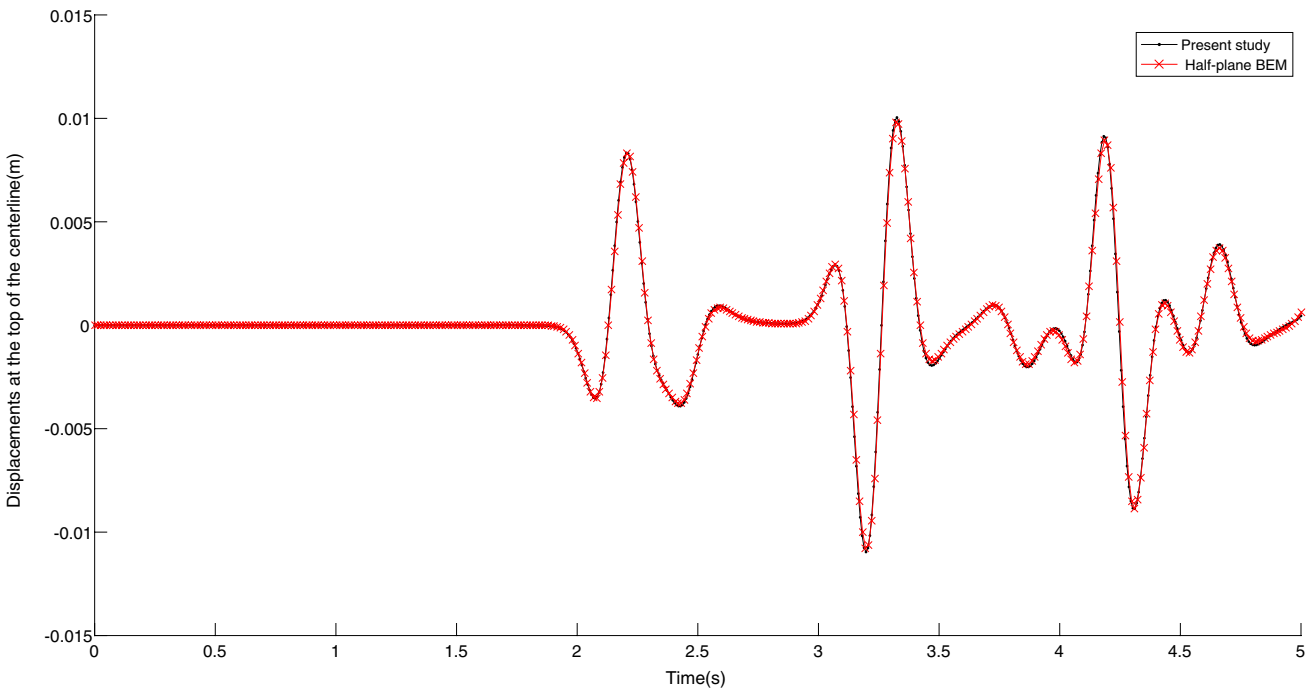

Fig. 9 Displacement time history in the central point on the ground surface at a velocity of 400 m/s with two FEM and half-plane BEM

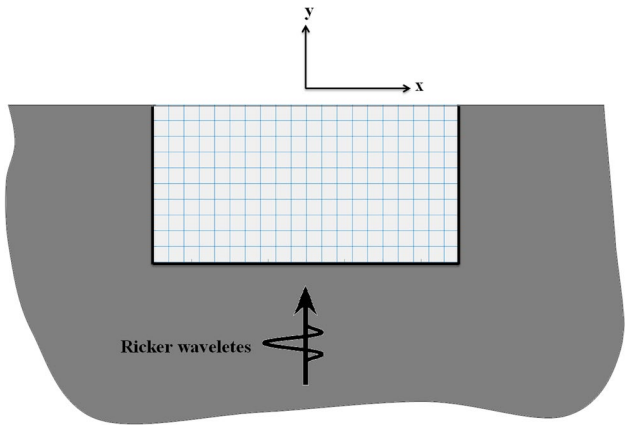

Fig. 10 Geometry and meshing the 2D site on rigid bedrock

Table 4 The analysis program of FEM to determine the proper length of the element

	c (m/s)	S (m)	N
1	400	25	5
2	400	16.67	8
3	400	12.5	10
4	400	10	13
5	400	7.14	18
6	700	50	4
7	700	25	9
8	700	16.67	14
9	700	12.5	18
10	600	50	4
11	600	33.333	6
12	600	25	8
13	600	12.5	16
14	600	10	20

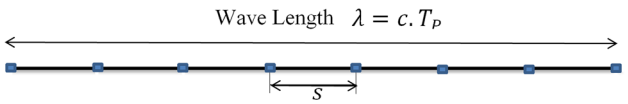

Fig. 11 Schematic layout of the parameters of Eq. 14

three shear wave velocities of 400, 600 and 700 m/s with the results of half-plane BEM. Soil density and Poisson ratio are considered to be $2\left(\mathrm{t}/\mathrm{m}^3\right)$ and 1/3, respectively, and information on the input SH wave such as time shift, predominant period, and the maximum amplitude of the displacement time history is assumed as 0.9 s, 1/3 s, and 0.001 m, respectively. In solving this problem, the eight-node second-order elements are used, and the Newmark's integration coefficients are $\alpha = 0.25$ and $\delta = 0.5$.

In Table 4, the analysis program of this problem is shown. The assumed time step of this analysis is 0.008 s and to select the proper length, the number of nodes in the smallest wavelength is measured (Eq. 14):

$$N = \frac{c \times T_{\mathrm{p}}}{S}, \tag{14}$$

where c is shear wave velocity, T_{p} is a predominant period, S is the distance between nodes, which is half of the element length, and N is the number of nodes on the smallest wavelength (Fig. 11).

The test results (Fig. 12) show three problems with velocities of 400, 600 and 700 m/s; if the length of the element is chosen in such a way that at least eight nodes are placed in the smallest wavelength, the results are obtained with acceptable accuracy and the results of the FEM match with those of the half-plane BEM. This conclusion is same as that suggested by Kuhlemeyer and Lysmer [38] for 1D site response analysis. Therefore, the maximum distance between nodes can be determined by the following equation:

$$S_{\max} = \frac{c \times T_{\mathrm{p}}}{8}. \tag{15}$$

6.2 Time Step

Selecting a proper time step is one of the effective parameters in calculating the accuracy of the results. This variable is not only effective on the accuracy of the results but also plays a key role in the volume of computations. To determine the optimal time step, first the maximum distance between nodes is calculated and then the β parameter is defined as Eq. 16 based on the velocity of shear wave c, time step Δt, and the maximum distance between nodes $S_{\max}$. This parameter shows the number of elements that passed through the seismic wave:

$$\beta = \frac{c \times \Delta t}{S_{\max}}. \tag{16}$$

By placing $S_{\max}$ equation in Eq. 16, the β parameter is simplified as follows. In this relation, β depends on the predominant period and time step:

$$\beta = \frac{8 \times \Delta t}{T_{\mathrm{p}}}. \tag{17}$$

The effect of this parameter is plotted at different velocities.

As seen in Fig. 13, for $\beta \leqslant 36\%$ the results obtained from FEM show good agreement with those of BEM. Since these results are independent of the shear wave velocity, the maximum time step can be obtained by replacing the maximum

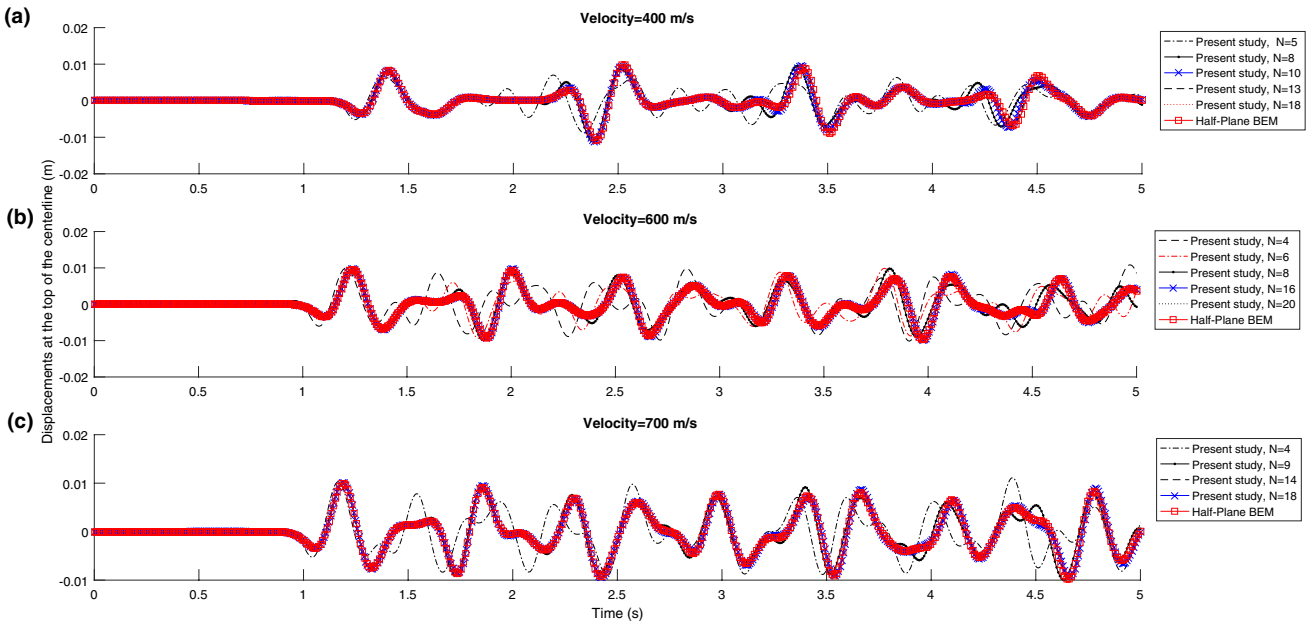

Fig. 12 The displacement time history in a central point on the ground surface with different element lengths

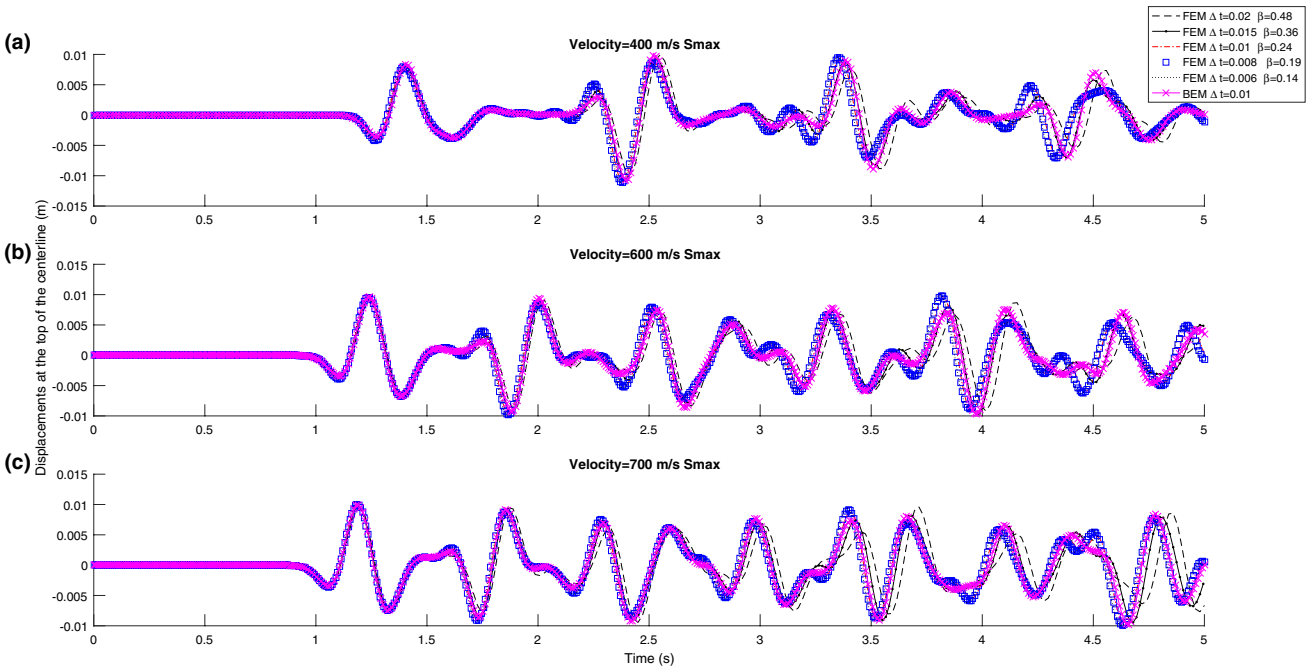

Fig. 13 Displacement time history in a central point on the ground surface with different time steps

value of β in Eq. 17. Equation 18 shows that the maximum time step is equivalent to $0.045T_p$:

$$\Delta t \leqslant 0.045T_p. \tag{18}$$

To verify Eqs. 15 and 18 in damping conditions, a one-dimensional example with dimensions 6000 m × 50 m is solved by assuming shear wave velocity of 300 m/s,

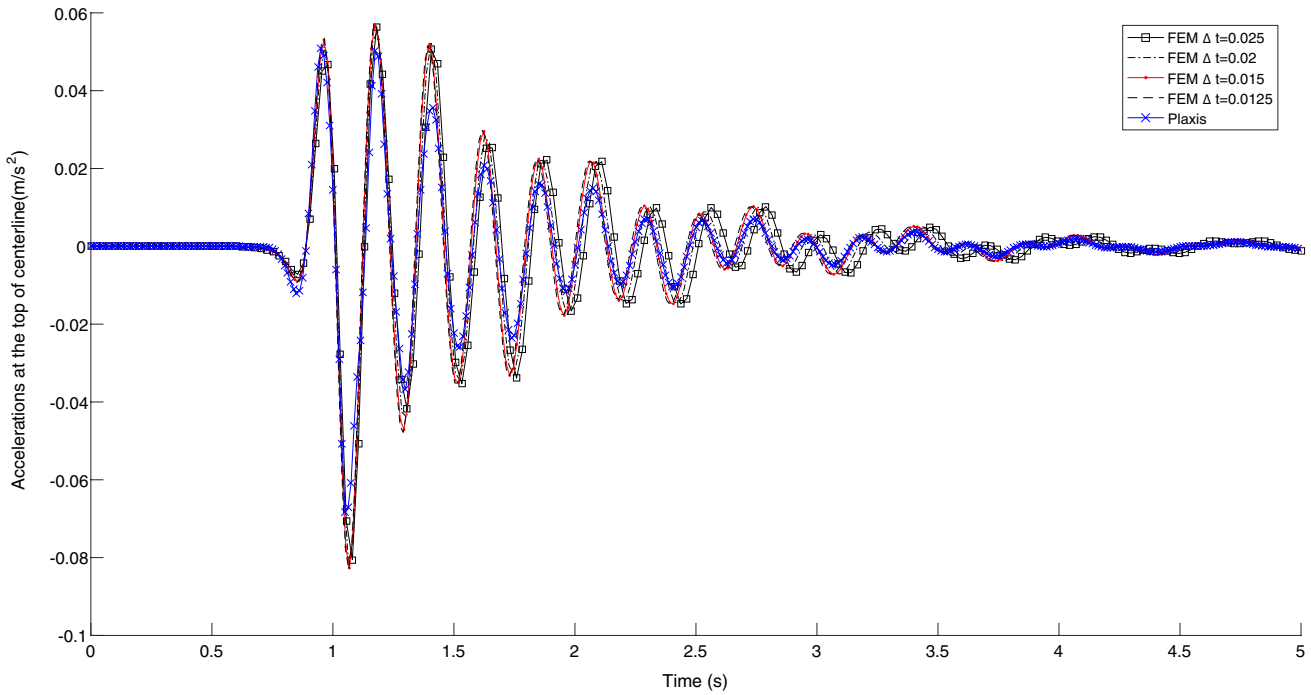

Fig. 14 The acceleration–time history in a central point on the ground surface at 300 m/s with maximum distance between the nodes in different time steps

predominant period of 1/3 s, time shift of 0.9 s and the maximum amplitude of the displacement time history of 0.0001 m. Using Eq. 15, the maximum distance between the nodes is calculated 12.5 m. The results are compared with Plaxis in different time steps. The analysis results in Fig. 14 show that there is a good agreement between the results at a time interval of 0.015 s. This is a time step equal to the proper time step of Eq. 18. Therefore, it can be said that the presented relationships for the length of the element and the appropriate time step can be generalized in the conditions of the damping of the materials.

6.3 Order of Numerical Integration

In numerical methods, the selection of integration method with proper ordering is one of the important issues. This selection has a significant effect on the cost of analysis and the accuracy of the result. Since in FEM stiffness, mass, surface, and volumetric forces are calculated by numerical integration method, in some studies, suggestions have been made in this regard. For instance, Bathe [36] proposed that in some cases to have more accurate mass matrix, it is possible to use a higher integration order in mass matrix compared to stiffness matrix. Therefore, in this section, the effect of the integral order is discussed.

In this program, a Gaussian integral method is used to calculate stiffness, mass, and force matrices. The program compares the results of this method at two different velocities of 400 and 700 m/s and with the damped and undamped materials. The damping ratio is assumed to be 0.05 in damped material conditions. In this comparison, three groups of integration order are chosen for the integral stiffness and mass matrices as follows:

1. Integration order of 3×3 (9 GPs) to the integration of stiffness and mass matrices.
2. Integration order of 3×3 (9 GPs) to the integration of stiffness matrix and integration order of 4×4 (16 GPs) to the integration of mass matrix.
3. Integration order of 4×4 (16 GPs) to the integration of stiffness and mass matrices.

The results in Fig. 15 indicate that in different conditions of velocity and damping of the material for eight-node elements, the integral order over 3 does not have an effect on the accuracy of the results, and choosing a higher order in integrating the mass matrix over the stiffness matrix does not increase the accuracy of the results.

6.4 Newmark's Integration Coefficients

In this study, the Newmark integration method is used to solve the problem. In this method which is indeed the expansion of the linear acceleration method, the choice of two

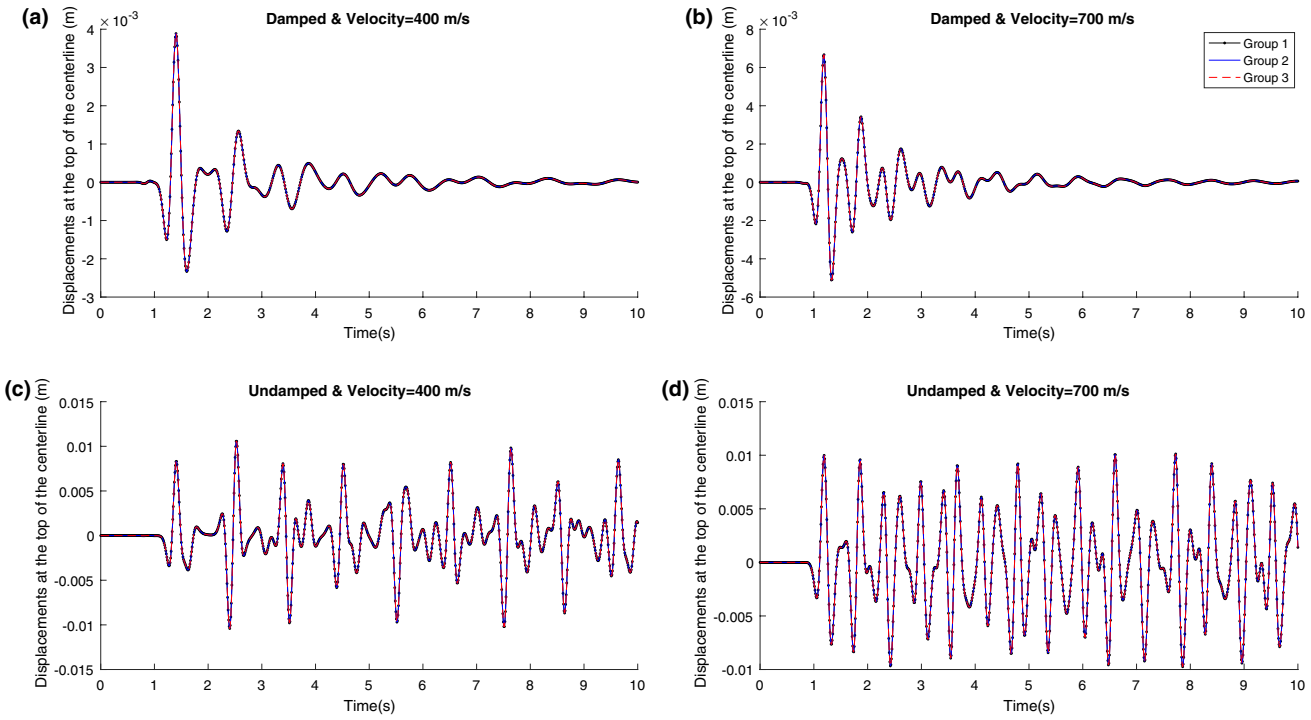

Fig. 15 Effect of the number of GPs on the displacement time history in the central point on the ground surface

Table 5 The FEM analysis plan for evaluating the effect of each of NCs

δ	0.5			0.6		
α	0.25	0.3025	0.4	0.25	0.3025	0.4

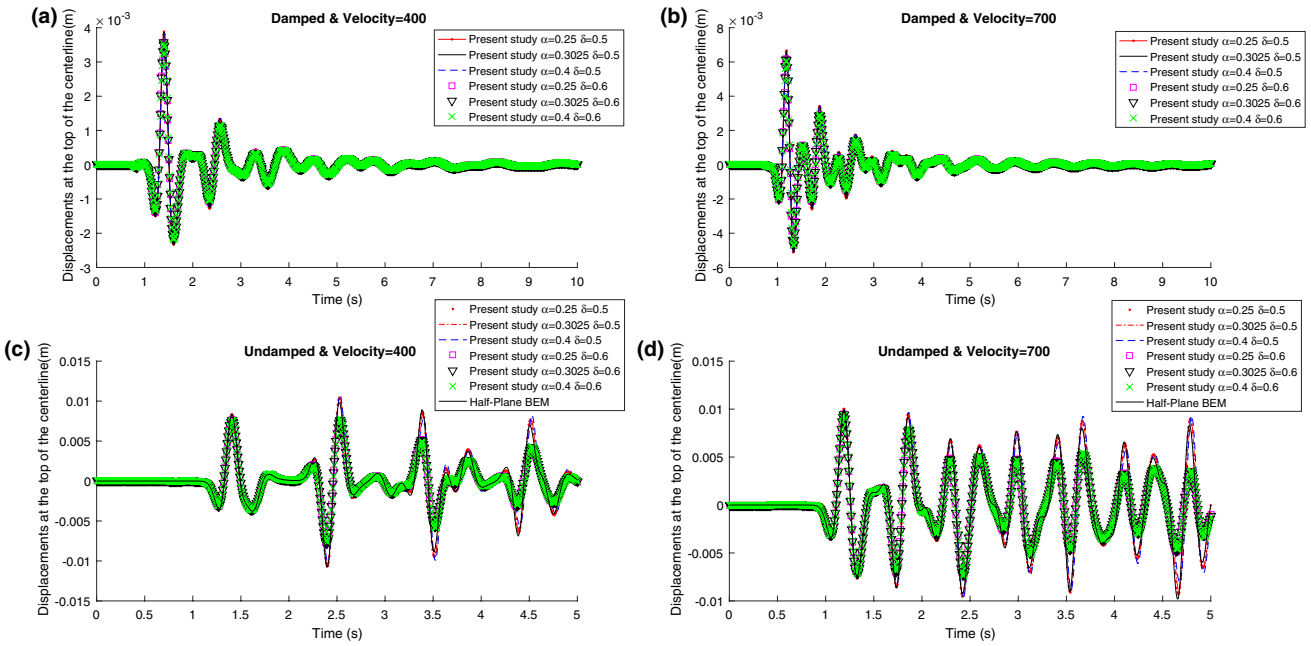

Fig. 16 Effect of NCs on the displacement time history in a central point on the ground surface

parameters α and δ plays a fundamental role in the accuracy of the integration and stability of the method. Considering the importance of achieving accurate results, in this section, we investigate the effect of these parameters on different velocities, damped, and undamped materials. For this purpose, six groups of NCs are used (Table 5). In the first three groups, the value of δ is equal to 0.5 and in the other three groups, δ is assumed to be 0.6. Also, the damping ratio is considered to be 5% in damped material conditions.

In Fig. 16, the results of solving the problem of SH wave propagation at two velocities of 400 and 700 m/s are shown. Comparison of the results of these six groups shows that the use of NCs of the second three groups in both damped and undamped conditions and at different velocities results in an amplitude drop. However, the difference is sharper in the undamped conditions. This result is in agreement with the explanations of Bathe [36] regarding the choice of $\delta > 0.5$ for the reduction of the amplitude.

Moreover, the use of NCs of the first three groups provides more favorable results, so that under undamped conditions, the results of FEM are consistent with those of half-plane BEM.

Another point that can be seen in Fig. 16 is that a change in α value at all conditions including damped, undamped, and various velocities has no effect on the results and only the value of δ as previously described, changes the results and reduces the amplitude.

6.5 Shape Ratio

In this section, the effect of alluvial valley geometry at 400 m/s shear wave velocity and 5% damping ratio is evaluated with mentioned properties of the input wave. The depth of alluvial valley is denoted with h, which is 75 m and half of the valley's width, b = 300, 150, 100, 75, 50, and 37.5 m. Shape ratio (SR) is defined as the ratio of depth to half width.

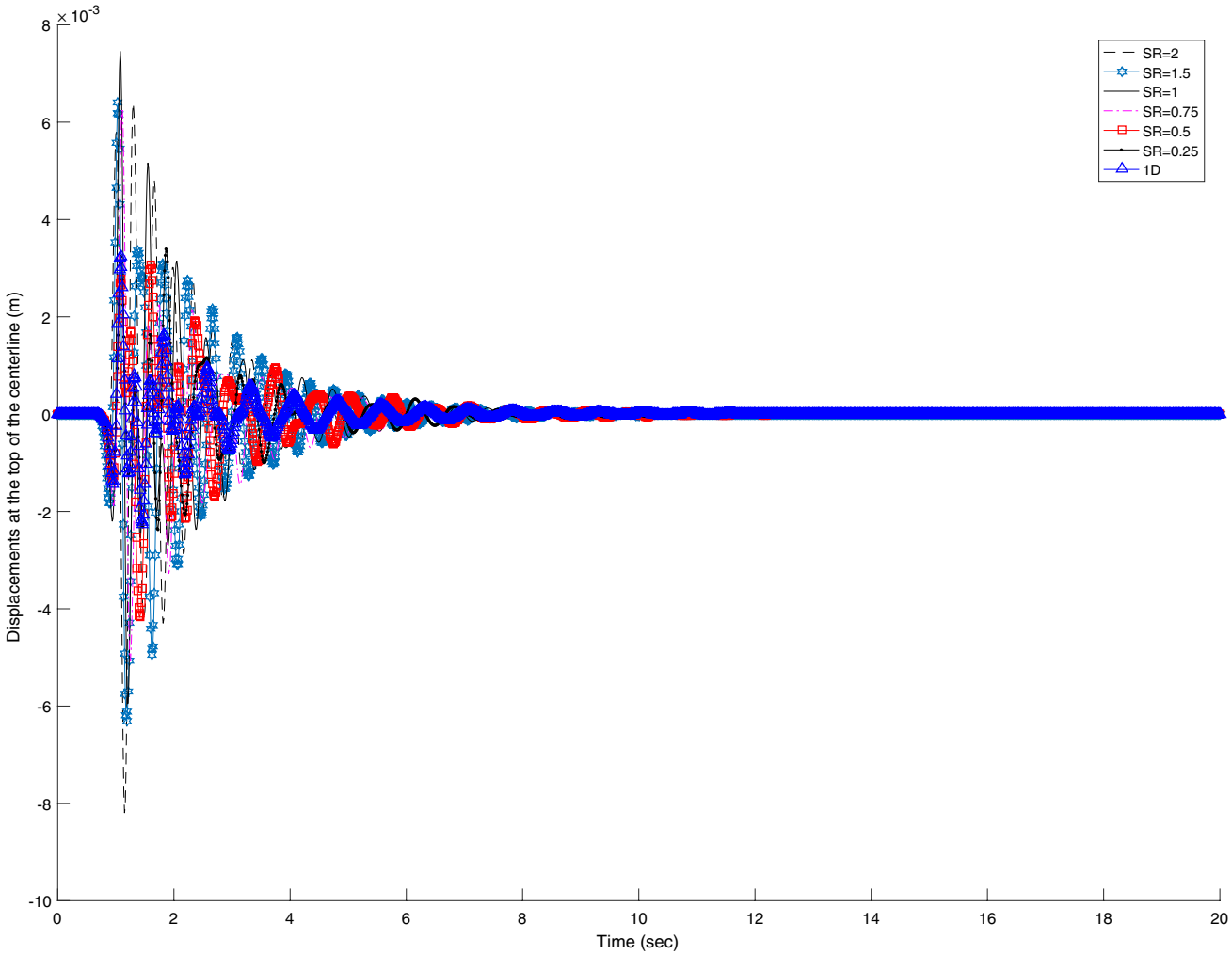

Fig. 17 The displacement time history in a central point on the ground surface in various SRs

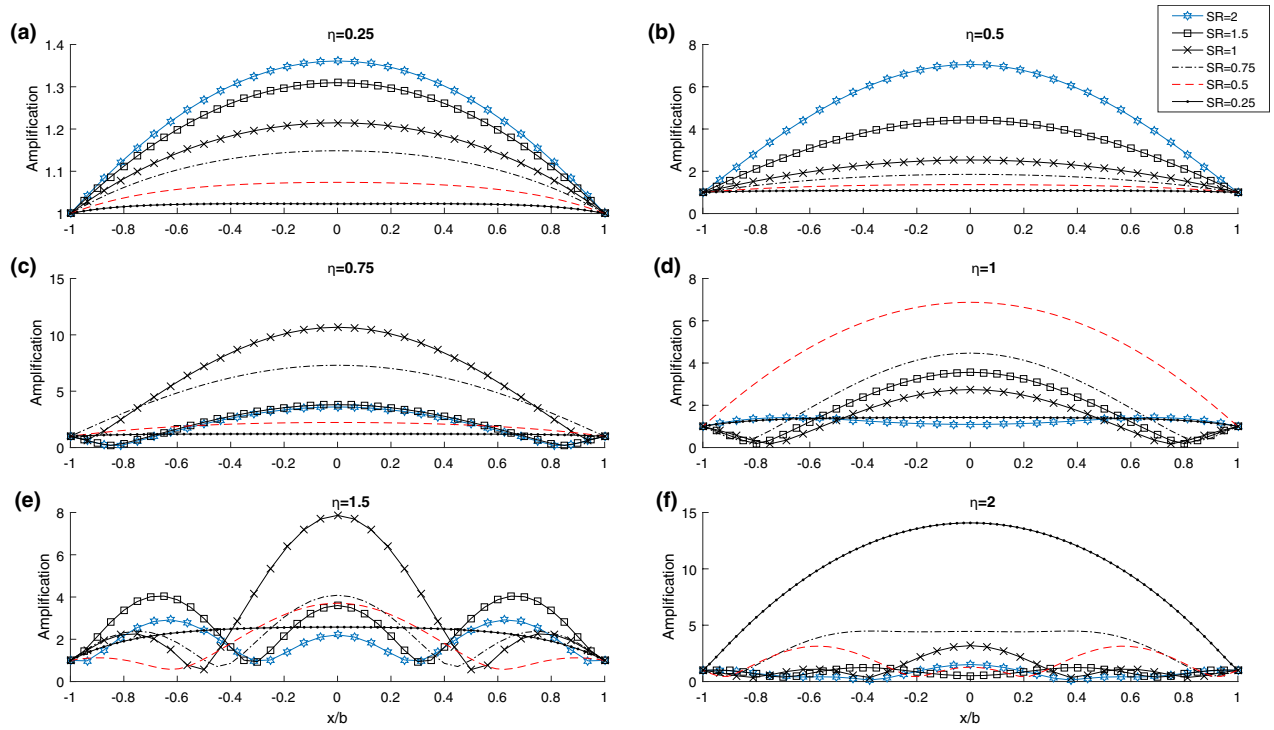

Fig. 18 Amplification variations in terms of SR along the rectangle-shaped alluvial valley

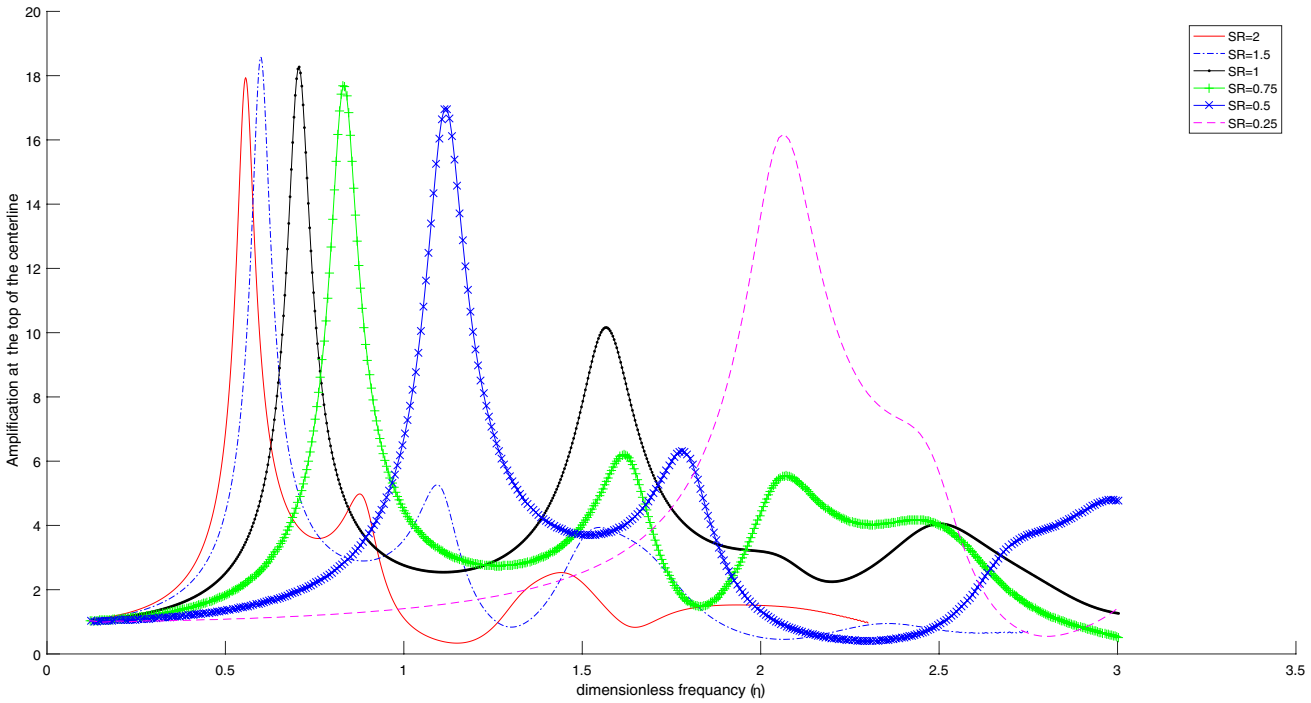

Fig. 19 Variations of the amplification curve at the top of the centerline of the rectangle-shaped alluvial valley in different SR

Figure 17 illustrates the displacement of the central point of the alluvial valley on the ground surface in various SR (0.25, 0.5, 0.75, 1, 1.5, and 2) compared with the displacement of the one-dimensional site. As shown in Fig. 17, a decrease in SR or reducing reduction in the depth of the valley leads to decrease in response amplitude so that in SR = 0.25, the response pattern is close to ground surface response of one-dimensional site.

Figures 18 and 19 present the amplification of valley surface in the frequency domain and various SRs. To present the results in this converted space, dimensionless frequency $\eta = \frac{\omega b}{\pi c}$ was defined, where η is dimensionless frequency, ω is the angular frequency of the incident wave, c is the velocity of the shear wave, and b is half width. As shown in figures, in very low frequencies, $\eta = 0.25$ amplification potential is negligible in various SRs. However, in low frequencies, amplification potential is significant in high SRs and by increasing the frequency, the amplification potential is increased in small SRs. It can show the reverse relationship of frequency and SR and a decrease in SR results in an increase in frequency (small wavelength). This result is in agreement with the results of other researchers that the significant effects of topography on seismic waves are observed when the incident wavelengths with the size of the topographic features are comparable [39–45]. In addition, in Fig. 19, the maximum amplification is 18.5, which is close to 29% lower than the Najafzadeh results [17] for the rectangular valley exposed to shear waves SV. This result demonstrates that SH shear waves have a smaller amplification than SV shear waves.

7 Conclusion

In the present study, an advanced formulation of FEM was presented for the 2D analysis of the seismic response of alluvial valleys located in a semi-infinite rigid space subjected to propagating incident SH waves in the time domain. The accuracy, efficiency, and ability of this formulation were demonstrated by analyzing the responsiveness of a 1D site and a 2D site. Then some numerical considerations in the dynamic analysis of this topographic feature were performed using parametric study on the seismic response of alluvial valley under propagating incident SH waves.

The results confirmed once again that

- the maximum distance between nodes should be equal to one-eighth of the smallest wavelength [38];
- the amplification ratio depends strongly on the shape ratio as well as the nondimensional frequency [17];
- the effect of a feature on the ground response is only noticeable if the wavelengths are comparable with the dimensions of the feature. If the dimensionless frequency is small (the wavelength of the incident wave is large), the effect of the feature will be significant only on the high SRs [39–45].

The results indicated, too, that

- if the maximum distance is between the nodes, the maximum value that can be selected as the time step is equal to 45/1000 of the predominant period of the incident wave;
- choosing a higher order in integrating the mass matrix has no effect on the accuracy of the results compared to stiffness matrix;
- the choice of $\delta > 0.5$ in Newmark's integration method reduces the amplitude, which is particulary evident in the results of the problems with the undamped materials;
- Of the two parameters of the NCs, only δ is effective in the results and a change in the α coefficient does not play a role in the accuracy of the results.

Acknowledgements This research was performed as a part of the PhD thesis of the author.

Funding The authors received no financial support for the research, authorship, and/ or publication of this article.

References

1. Trifunac MD (1971) Surface motion of a semi-cylindrical alluvial valley for incident plane SH waves. Bull Seismol Soc Am 61(6):1755–1770
2. Wong HL, Trifunac MD (1974) Surface motion of a semi-elliptical alluvial valley for incident plane SH waves. Bull Seismol Soc Am 64(5):1389–1408
3. Bard PY, Bouchon M (1985) The two-dimensional resonance of sediment-filled valleys. Bull Seismol Soc Am 75(2):519–541
4. Todorovska MI, Lee VW (1991) Surface motion of shallow circular alluvial valleys for incident plane SH waves-analytical solution. Soil Dyn Earthq Eng 10(4):192–200
5. Chen JT, Chen PY, Chen CT (2008) Surface motion of multiple alluvial valleys for incident plane SH-waves by using a semi-analytical approach. Soil Dyn Earthq Eng 28(1):58–72
6. Jaramillo J, Gomez J, Saenz M, Vergara J (2012) Analytic approximation to the scattering of antiplane shear waves by free surfaces of arbitrary shape via superposition of incident, reflected and diffracted rays. Geophys J Int 192(3):1132–1143
7. Kara HF, Trifunac MD (2014) Two-dimensional earthquake vibrations in sedimentary basins—SH waves. Soil Dyn Earthq Eng 63:69–82
8. Le T, Lee VW, Trifunac MD (2017) SH waves in a moon-shaped valley. Soil Dyn Earthq Eng 101:162–175
9. Tsaur DH, Chang KH (2008) SH-waves scattering from a partially filled semi-circular alluvial valley. Geophys J Int 173(1):157–167
10. Tsaur DH, Chang KH (2009) Scattering of SH waves by truncated semicircular canyon. J Eng Mech ASCE 135(8):862–870

11. Tsaur DH, Chang KH, Hsu MS (2010) An analytical approach for the scattering of SH waves by a symmetrical V-shaped canyon: deep case. Geophys J Int 183(3):1501–1511
12. Tsaur DH, Hsu MS (2013) SH waves scattering from a partially filled semi-elliptic alluvial valley. Geophys J Int 194(1):499–511
13. Eringen AC, Suhubi ES (1975) Elastodynamics. Academic, London
14. Chuhan Z, Chongbin Z (1988) Effects of canyon topography and geological conditions on strong ground motion. Earthq Eng Struct Dyn 16(1):81–97
15. Zhao C, Valliappan S (1993) Incident P and SV wave scattering effects under different canyon topographic and geological conditions. Int J Numer Anal Methods Geomech 17(2):73–94
16. Chaljub E, Komatitsch D, Vilotte JP, Capdeville Y, Valette B, Festa G (2007) Spectral-element analysis in seismology. Adv Geophys 48:365–419
17. Najafizadeh J, Kamalian M, Jafari MK, Khaji N (2014) Seismic analysis of rectangular alluvial valleys subjected to incident SV waves by using the spectral finite element method. Int J Civ Eng 12(3):251–263
18. Aminpour P, Najafizadeh J, Kamalian M, Jafari MK (2015) Seismic response of 2D triangular-shaped alluvial valleys to vertically propagating incident SV waves. J Seismol Earthq Eng 17(2):89–101
19. Bielak J, Xu J, Ghattas O, Member A, Xu J, Ghattas O (1999) Earthquake ground motion and structural response in alluvial valleys. J Geotech Geoenviron Eng ASCE 125(5):413–423
20. Gelagoti F, Kourkoulis R, Anastasopoulos I, Tazoh T, Gazetas G (2010) Seismic wave propagation in a very soft alluvial valley: sensitivity to ground-motion details and soil nonlinearity, and generation of a parasitic vertical component. Bull Seismol Soc Am 100(6):3035–3054
21. Takemiya H, Fujiwara A (1994) SH-wave scattering and propagation analyses at irregular sites by time domain BEM. Bull Seismol Soc Am 84(5):1443–1455
22. Fishman KL, Ahmad S (1995) Seismic response for alluvial valleys subjected to SH, P and SV waves. Soil Dyn Earthq Eng 14(4):249–258
23. Semblat JF, Kham M, Parara E, Bard PY, Pitilakis K, Makra K et al (2005) Seismic wave amplification: Basin geometry vs soil layering. Soil Dyn Earthq Eng 25(7–10):529–538
24. Dravinski M (2007) Scattering of waves by a sedimentary basin with a corrugated interface. Bull Seismol Soc Am 97(1B):256–264
25. Luzón F, Sánchez-Sesma FJ, Pérez-Ruiz JA, Ramírez-Guzmán L, Pech A (2009) In-plane seismic response of inhomogeneous alluvial valleys with vertical gradients of velocities and constant Poisson ratio. Soil Dyn Earthq Eng 29(6):994–1004
26. Omidvar B, Rahimian M, Mohammadnejad T, Sanaeiha A (2010) Three-dimensional scattering of plane harmonic SH, SV, and P waves in multilayered alluvial valleys. Asian J Civ Eng 11(5):605–626
27. Delépine N, Semblat JF (2012) Site effects in an alpine valley with strong velocity gradient: interest and limitations of the "classical" BEM". Soil Dyn Earthq Eng 38:15–24
28. Kham M, Semblat JF, Bouden-Romdhane N (2013) Amplification of seismic ground motion in the Tunis basin: numerical BEM simulations vs experimental evidences. Eng Geol 155:80–86
29. Panji M, Kamalian M, Marnani JA, Jafari MK (2013) Transient analysis of wave propagation problems by half-plane BEM. Geophys J Int 194(3):1849–1865
30. Panji M, Kamalian M, Marnani JA, Jafari MK (2014) Antiplane seismic response from semi-sine shaped valley above embedded truncated circular cavity: a time-domain half-plane BEM. Int J Civ Eng 12(2):193–206
31. Panji M, Kamalian M, Marnani JA, Jafari MK (2014) Analysing seismic convex topographies by a half-plane time-domain BEM. Geophys J Int 197(1):591–607
32. Bielak J, MacCamy RC, MacGhess DS, Barry A (1991) Unified symmetric BEM-FEM for site effects on ground motion-SH waves. J Eng Mech ASCE 117(10):2265–2285
33. Gil-Zepeda SA, Montalvo-Arrieta JC, Vai R, Sánchez-Sesma FJ (2003) A hybrid indirect boundary element—discrete wave number method applied to simulate the seismic response of stratified alluvial valleys. Soil Dyn Earthq Eng 23(1):77–86
34. Shyu WS, Teng TJ, Chou CS (2016) Anti-plane response induced by an irregular alluvial valley using a hybrid method with modified transfinite interpolation. Soil Dyn Earthq Eng 90:250–264
35. Dominguez J (1993) Boundary elements in dynamics. Computational Mechanics Publications, Southampton
36. Bathe KJ (1982) Finite element procedures in engineering analysis. Prentice-Hall, Englewood Cliffs
37. Desai CS, Christian JT (1979) Numerical methods in geotechnical engineering. McGraw-Hill, New York
38. Kuhlemeyer RL, Lysmer J (1973) Finite element method accuracy for wave propagation problems. J Soil Mech Found Div 99(5):421–427
39. Bouchon M (1973) Effect of topography on surface motion. Bull Seismol Soc Am 63(2):615–632
40. Boore DM (1972) A note on the effect of simple topography on seismic SH waves. Bull Seismol Soc Am 62(1):275–284
41. Boore DM, Harmsen SC, Harding ST (1981) Wave scattering from a step change in surface topography. Bull Seismol Soc Am 71(1):117–125
42. Bard PY (1982) Diffracted waves and displacement field over two-dimensional elevated topographies. Geophys J Int 71(3):731–760
43. Sanchez-Sesma FJ (1983) Diffraction of elastic waves by three-dimensional surface irregularities. Bull Seismol Soc Am 73(6A):1621–1636
44. Geli L, Bard PY, Jullien B (1988) The effect of topography on earthquake ground motion: a review and new results. Bull Seismol Soc Am 78(1):42–63
45. Sánchez-Sesma FJ, Eduardo Pérez-Rocha L, Chávez-Pérez S (1989) Diffraction of elastic waves by three-dimensional surface irregularities. Part II. Bull Seismol Soc Am 79(1):101–112